Hindawi
Advances in High Energy Physics
Volume 2017, Article ID 1248563, 15 pages
https://doi.org/10.1155/2017/1248563

Review Article

A Review of Elliptic Flow of Light Nuclei in Heavy-Ion Collisions at RHIC and LHC Energies

Md. Rihan Haque,[1] Chitrasen Jena,[2,3] and Bedangadas Mohanty[2]

[1] *Utrecht University, P.O. Box 80000, 3508 TA Utrecht, Netherlands*
[2] *School of Physical Sciences, National Institute of Science Education and Research, Jatni 752050, India*
[3] *Indian Institute of Science Education and Research, Tirupati 517507, India*

Correspondence should be addressed to Md. Rihan Haque; r.haque@uu.nl

Received 30 June 2016; Revised 27 September 2016; Accepted 29 May 2017; Published 15 August 2017

Academic Editor: Shi-Hai Dong

We present a review of the measurements of elliptic flow (v_2) of light nuclei (d, $\bar{d}$, t, ^{3}He, and $^3\overline{\text{He}}$) from the RHIC and LHC experiments. Light (anti)nuclei v_2 have been compared with that of (anti)proton. We observed a similar trend in light nuclei v_2 to that in identified hadron v_2 with respect to the general observations such as p_T dependence, low p_T mass ordering, and centrality dependence. We also compared the difference of nuclei and antinuclei v_2 with the corresponding difference of v_2 of proton and antiproton at various collision energies. Qualitatively they depict similar behavior. We also compare the data on light nuclei v_2 to various theoretical models such as blast-wave and coalescence. We then present a prediction of v_2 for ^{3}He and ^{4}He using coalescence and blast-wave models.

1. Introduction

The main goals of high energy heavy-ion collision experiments have primarily been to study the properties of Quark Gluon Plasma (QGP) and the other phase structures in the QCD phase diagram [1–11]. The energy densities created in these high energy collisions are similar to that found in the universe, microseconds after the Big Bang [5–8, 12–14]. Subsequently, the universe cooled down to form nuclei. It is expected that high energy heavy-ion collisions will allow studying the production of light nuclei such as d, t, ^{3}He, and their corresponding antinuclei. There are two possible production mechanisms for light (anti)nuclei. The first mechanism is thermal production of nucleus-antinucleus pairs in elementary nucleon-nucleon or parton-parton interactions [15–21]. However, due to their small (~ few MeV) binding energies, the directly produced nuclei or antinuclei are likely to break up in the medium before escaping. The second mechanism is via final state coalescence of produced (anti)nucleons or from transported nucleons [22–36]. The quark coalescence as a mechanism of hadron production at intermediate transverse momentum has been well established by studying the number of constituent quarks (NCQ) scaling for v_2 of identified hadrons measured at RHIC [37–45]. Light nuclei may also be produced via coalescence of quarks similar to the hadrons. But the nuclei formed via quark coalescence are highly unlikely to survive in the high temperature environment due to their small binding energies. In case of hadron formation by quark coalescence, the momentum space distribution of quarks is not directly measurable in experiments. However, in case of nucleon coalescence, momentum space distributions of both the constituents (nucleons) and the products (nuclei) are measurable in heavy-ion collision experiments. Therefore, measurements of v_2 of light nuclei provide a tool to understand the production mechanism of light nuclei and freeze-out properties at a later stage of the evolution. It also provides an excellent opportunity to understand the mechanism of coalescence at work in high energy heavy-ion collisions.

The production of light (anti)nuclei has been studied extensively at lower energies in Bevelac at LBNL [24, 46–49], AGS at RHIC [50–53], and SPS at CERN [54–58]. In the AGS

experiments, it was found that the coalescence parameter (B_2) is of similar magnitude for both d and $\overline{d}$ indicating similar freeze-out hypersurface of nucleons and antinucleons. Furthermore, the dependence of B_2 on collision energy and p_T indicated that light nuclei production is strongly influenced by the source volume and transverse expansion profile of the system [58, 59]. In this paper, we review the results of elliptic flow of light nuclei measured at RHIC and LHC and discuss the possible mechanisms for the light nuclei production.

The paper is organized as follows. Section 2 briefly describes the definition of v_2, identification of light (anti)nuclei in the experiments and measurement of v_2 of light (anti)nuclei. In Section 3, we present the v_2 results for minimum bias collisions from various experiments. We also discuss the centrality dependence, difference between nuclei and antinuclei v_2, and the energy dependence of deuteron v_2. In the same section, we present the atomic mass number scaling and also compare the experimental results with various theoretical models. Finally in Section 4, we summarize our observations and discuss the main conclusions of this review.

2. Experimental Method

2.1. Elliptic Flow (v_2). The azimuthal distribution of produced particles in heavy-ion collision can be expressed in terms of a Fourier series,

$$\frac{dN}{d\left(\phi - \Psi_r\right)} \propto 1 + \sum_n 2v_n \cos\left[n\left(\phi - \Psi_r\right)\right], \tag{1}$$

where ϕ is the azimuthal angle of produced particle, Ψ_r is called the reaction plane angle, and the Fourier coefficients v_1, v_2, and so on are called flow coefficients [60]. Ψ_r is defined as the angle between the impact parameter vector and the x-axis of the reference detector in the laboratory frame. Since it is impossible to measure the direction of impact parameter in heavy-ion collisions, a proxy of Ψ_r, namely, the event plane angle Ψ_n, is used for the flow analysis in heavy-ion collisions [61]. v_2 is measured with respect to the 2nd-order event plane angle Ψ_2 [61]. Ψ_2 is calculated using the azimuthal distribution of the produced particles. In an event with N particles, the event plane angle Ψ_2 is defined as [61]

$$\Psi_2 = \frac{1}{2}\tan^{-1}\left(\frac{Y_2}{X_2}\right). \tag{2}$$

X_2 and Y_2 are defined as

$$X_2 = \sum_{i=1}^{N} w_i \cos\left(2\phi_i\right), \tag{3a}$$

$$Y_2 = \sum_{i=1}^{N} w_i \sin\left(2\phi_i\right), \tag{3b}$$

where w_i are weights given to each particle to optimise the event plane resolution [61, 62]. Usually the magnitude of particle transverse momentum p_T is used as weights as v_2 increases with p_T. Special techniques are followed while calculating the event plane angle so that it does not contain the particle of interest whose v_2 is to be calculated (self-correlation) and also the nonflow effects (e.g., jets and short range correlations) are removed as much as possible [41, 42, 61, 63]. Heavy-ion experiments use the η-subevent plane method to calculate the elliptic flow of identified hadrons as well as for light nuclei. In this method, each event is divided into two subevents in two different η-windows (e.g., positive and negative η). Then two subevent plane angles are calculated with the particles in each subevent. Each particle with a particular η is then correlated with the subevent plane of the opposite η. This ensures that the particle of interest is not included in the calculation of event plane angle. A finite η gap is applied between the two subevents to reduce short range correlations which does not originate from flow.

The distribution of the event plane angles should be isotropic in the laboratory frame for a azimuthally isotropic detector. If the distribution of the event plane angles is not flat in the laboratory frame (due to detector acceptance and/or detector inefficiency) then special techniques are applied to make the distribution uniform. The popular methods to make the Ψ_2 distribution uniform is the ϕ-weight and recentering [64, 65]. In the ϕ-weight method, one takes the actual azimuthal distribution of the produced particle, averaged over large sample of events, and then uses inverse of this distribution as weights while calculating the correlation of the particles with the event plane angle [64, 65]. In the recentering method, one subtracts $\langle X_n \rangle$ and $\langle Y_n \rangle$ from the event-by-event X_n and Y_n, respectively, where $\langle X_n \rangle$ and $\langle Y_n \rangle$ denote the average of X_n and Y_n over a large sample of similar events. The main disadvantage of applying one of these methods is that it does not remove the contribution from higher flow harmonics. Therefore, another correction method known as the shift correction is used to remove the effects coming from higher flow harmonics. In this method, one fits the Ψ_2 distribution (after applying ϕ-weight and/or recentering method) averaged over all events, with a Fourier function. The Fourier coefficients from this fit (obtained as fit parameters) are used to shift Ψ_2 of each event, to make the distribution uniform in the laboratory frame [64, 65].

Since the number of particles produced in heavy-ion collisions are finite, the calculated event plane angle Ψ_2 may not coincide with Ψ_r. For this reason, the measured v_2^{obs} with respect to Ψ_2 is corrected with the event plane resolution factor R_2, where

$$R_2 = \left\langle \cos\left[2\left(\Psi_2 - \Psi_r\right)\right]\right\rangle. \tag{4}$$

In order to calculate the event plane resolution, one calculates two subevent plane angles Ψ_2^a and Ψ_2^b, where a and b correspond to two independent subevents. If the multiplicities of each subevent are approximately half of the full event plane, then the resolution of each of subevent plane can be calculated as [60, 61],

$$\left\langle \cos\left[2\left(\Psi_2^a - \Psi_r\right)\right]\right\rangle = \sqrt{\left\langle \cos\left[2\left(\Psi_2^a - \Psi_2^b\right)\right]\right\rangle}. \tag{5}$$

Table 1: Available measurements of light nuclei v_2.

Experiment	Nuclei	$\sqrt{s_{NN}}$ (GeV)	Centrality
STAR [63]	$d, \bar{d}, t,$ ^{3}He, $^3\overline{\text{He}}$	7.7, 11.5, 19.6, 27, 39, 62.4, 200	0–80%, 0–30%, 30–80% (0–10%, 10–40%, 40–80% in 200 GeV)
PHENIX [66]	$d + \bar{d}$	200	0–20%, 20–60%
ALICE [67]	$d + \bar{d}$	2760	0–5%, 5–10%, 10–20%, 20–30%, 30–40%, 40–50%

However, the full event plane resolution can be expressed as

$$\left\langle \cos\left[2\left(\Psi_2 - \Psi_r\right)\right]\right\rangle = \frac{\sqrt{\pi}}{2\sqrt{2}}\chi_2 \exp\left(-\frac{\chi_2^2}{4}\right) \times \left[I_0\left(\frac{\chi_2^2}{4}\right) + I_2\left(\frac{\chi_2^2}{4}\right)\right], \quad (6)$$

where $\chi_2 = v_2/\sigma$ and I_0, I_2 are modified Bessel functions [60, 61]. The parameter σ is inversely proportional to the square-root of N, the number of particles used to determine the event plane [60, 61]. To calculate the resolution for full event plane (Ψ_2), one has to solve (6) iteratively for the value of χ_2 using the subevent plane resolution ($\langle\cos[2(\Psi_2^a - \Psi_r)]\rangle$) which is calculated experimentally using (5). The χ_2 value is then multiplied with $\sqrt{2}$ as χ_2 is proportional to $\sqrt{N}$ and reused in (6) to calculate the resolution of the full event plane. In a case of very low magnitudes, the full event plane resolution can be approximately given as [60, 61]

$$\begin{aligned}\left\langle \cos\left[2\left(\Psi_2 - \Psi_r\right)\right]\right\rangle &= \sqrt{2}\left\langle \cos\left[2\left(\Psi_2^a - \Psi_r\right)\right]\right\rangle \\ &= \sqrt{2\left\langle \cos\left[2\left(\Psi_2^a - \Psi_2^b\right)\right]\right\rangle}.\end{aligned} \quad (7)$$

The procedure for calculating full and subevent plane resolutions using subevent plane angles and various approximations is discussed in detail in [60, 61].

2.2. Data on Light Nuclei. For this review, we have collected light nuclei v_2 data from the STAR [63] and PHENIX [66] experiments at RHIC and ALICE experiment at LHC [67]. Table 1 summarizes the measurement of light nuclei v_2 available till date.

2.3. Extraction of Light Nuclei v_2. In heavy-ion collisions, light nuclei are primarily identified by comparing the mean ionization energy loss per unit length ($\langle dE/dx\rangle$) in the Time Projection Chamber (TPC) with that from the theoretical predictions ($dE/dx|_{\text{theo}}$) [41, 42, 63, 67–71]. Light nuclei are also identified via the time-of-flight measurement techniques using the Time-of-Flight (TOF) detector [66, 67, 71–74].

In the STAR experiment, to identify light nuclei using TPC, a variable Z [63] is defined as

$$Z = \log\left[\frac{\langle dE/dx\rangle}{(dE/dx)}\bigg|_{\text{theo}}\right]. \quad (8)$$

Then the light nuclei yields are extracted from these Z-distributions in differential p_T and $(\phi - \Psi_2)$ bins either for minimum bias collisions or in selected centrality classes. The $(\phi - \Psi_2)$ distribution is then fitted with a 2nd-order Fourier function; namely,

$$\frac{dN}{d\left(\phi - \Psi_2\right)} \sim 1 + 2v_2\cos\left(\phi - \Psi_2\right). \quad (9)$$

The Fourier coefficient v_2 is called elliptic flow and is extracted from the fit. As we discussed in the previous subsection this measured v_2 is then corrected with the event plane resolution factor (R_2) [41, 42, 63].

In the ALICE experiment, light nuclei in the low p_T region (<1.0 GeV/c for d, $\bar{d}$) are identified by comparing the variance ($\sigma_{\langle dE/dx\rangle}$) of the measured $\langle dE/dx\rangle$ in the TPC with the corresponding theoretical estimate ($dE/dx|_{\text{theo}}$) [67, 71]. Light nuclei are considered identified if the measured $\langle dE/dx\rangle$ lies within $\pm 3\sigma_{\langle dE/dx\rangle}$ of the $dE/dx|_{\text{theo}}$. On the other hand, the light nuclei yield is extracted from the mass squared (m^2_{TOF}) distribution using the TOF detector. The mass of each particle is calculated using the time-of-flight (t) from the TOF detector and the momentum ($\mathbf{p}$) information from the TPC [66, 67, 71]. Both the ALICE and PHENIX experiments use the TOF detector to identify light nuclei at high p_T (>1.0 GeV/c). The mass of a particle can be calculated using the TOF detector as

$$m^2_{\text{TOF}} = \frac{\mathbf{p}^2}{c^2}\left(\frac{c^2t^2}{L^2} - 1\right), \quad (10)$$

where the track length L and momentum $\mathbf{p}$ are determined with the tracking detectors placed inside magnetic field [44, 66, 67, 71]. After getting m^2 for each particle, a selection cut is implemented to reject tracks which have their m^2 several σ away from the true m^2 value of the light nuclei, as done in the STAR experiment [63]. The ALICE experiment, on the other hand, defines a quantity Δm such that $\Delta m = m_{\text{TOF}} - m_{\text{nucl}}$, where m_{nucl} is the mass of the light nuclei under study. The distribution of Δm is then fitted with a Gaussian + exponential function for signal and an exponential function for the background [67]. Then v_2 of light nuclei is calculated by fitting $v_2(\Delta m)$ with the weighted function,

$$\begin{aligned}v_2^{\text{Tot}}(\Delta m) = {} & v_2^{\text{Sig}}(\Delta m)\frac{N^{\text{Sig}}}{N^{\text{Tot}}}(\Delta m) \\ & + v_2^{\text{Bkg}}(\Delta m)\frac{N^{\text{Bkg}}}{N^{\text{Tot}}}(\Delta m),\end{aligned} \quad (11)$$

where the total measured v_2^{Tot} is the weighted sum of that from the signal (v_2^{Sig}) and background (v_2^{Bkg}). v_2^{Tot} of the candidate

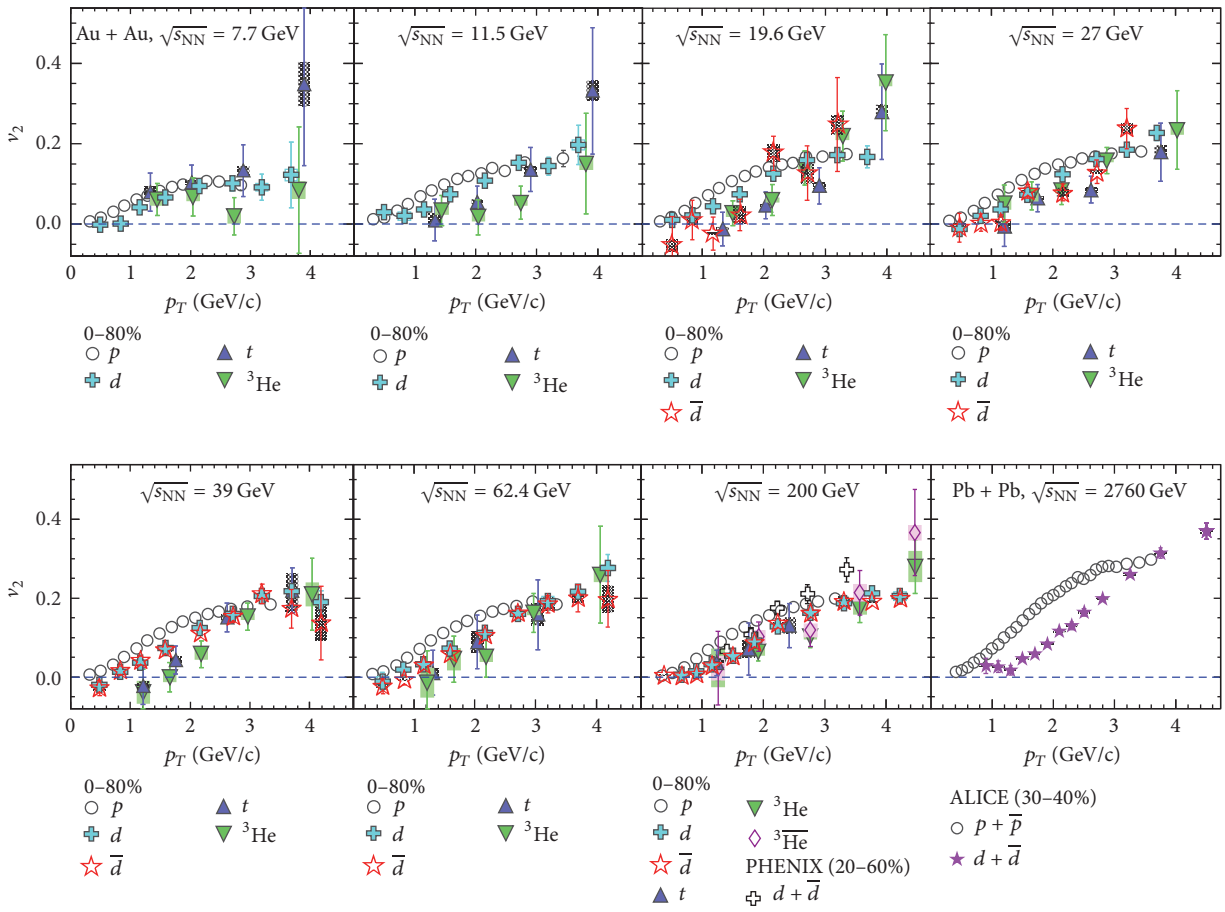

FIGURE 1: Midrapidity $v_2(p_T)$ for light nuclei (d, $\overline{d}$, t, ^{3}He, and $^3\overline{\text{He}}$) in 0–80%, 20–60%, and 30–40% centrality from STAR, PHENIX, and ALICE, respectively. Proton $v_2(p_T)$ is also shown as open circles [41–44, 75] for comparison. Lines and boxes at each marker corresponds to statistical and systematic errors, respectively.

particles are calculated using the scalar product method and corrected for the event plane resolution [67].

The PHENIX experiment calculates charged average v_2 of (anti) deuterons as

$$v_2 = \frac{\langle \cos\left(2\left(\phi - \Psi_2\right)\right)\rangle}{R_2}. \tag{12}$$

The quantity $R_2 = \langle \cos(2(\Psi_2 - \Psi_r))\rangle$ can readily be identified as the resolution of the event plane angle [66]. The resolution of full event plane Ψ_2 is calculated with subevent planes (Ψ_2^a, Ψ_2^b) estimated using two Beam-Beam Counter (BBC) detectors [44, 66]. The detailed procedure of calculating the full event plane resolution from subevents is already mentioned in the previous subsection. The large η gap between the central TOF and the BBCs ($\Delta\eta > 2.75$) reduces the effects of nonflow significantly [44, 66]. The nuclei v_2 calculated in PHENIX are also corrected for the contribution coming from backgrounds, mainly consisting of misidentification of other particles (e.g., protons) as nuclei. A p_T dependent correction factor was applied on the total v_2 (referred to as $v_2^{\text{Sig+Bkg}}(p_T)$) such that

$$v_2^{d(\overline{d})}\left(p_T\right) = \frac{\left[v_2^{\text{Sig+Bkg}}\left(p_T\right) - (1-R)\, v_2^{\text{Bkg}}\left(p_T\right)\right]}{R}, \tag{13}$$

where $v_2^{\text{Sig+Bkg}}(p_T)$ is the measured v_2 for $d(\overline{d})$ + background at a given p_T, $v_2^{d(\overline{d})}$ is the corrected v_2 of $d(\overline{d})$, and R is the ratio of signal and signal + background.

3. Results and Discussion

3.1. General Aspects of Light Nuclei v_2. Figure 1 shows the energy dependence of light (anti)nuclei v_2 for $\sqrt{s_{NN}}$ = 7.7, 11.5, 19.6, 27, 39, 62.4, 200, and 2760 GeV. The panels are arranged by increasing energy from left to right and top to bottom. The p_T dependence of v_2 of d, $\overline{d}$, t, ^{3}He, and $^3\overline{\text{He}}$ is shown for 0–80% centrality in STAR, 20–60% centrality in PHENIX, and 30–40% centrality in ALICE. Since PHENIX and ALICE do not have measurements in the minimum bias collisions, we only show the results for mid-central collisions. The data points of PHENIX and ALICE correspond to

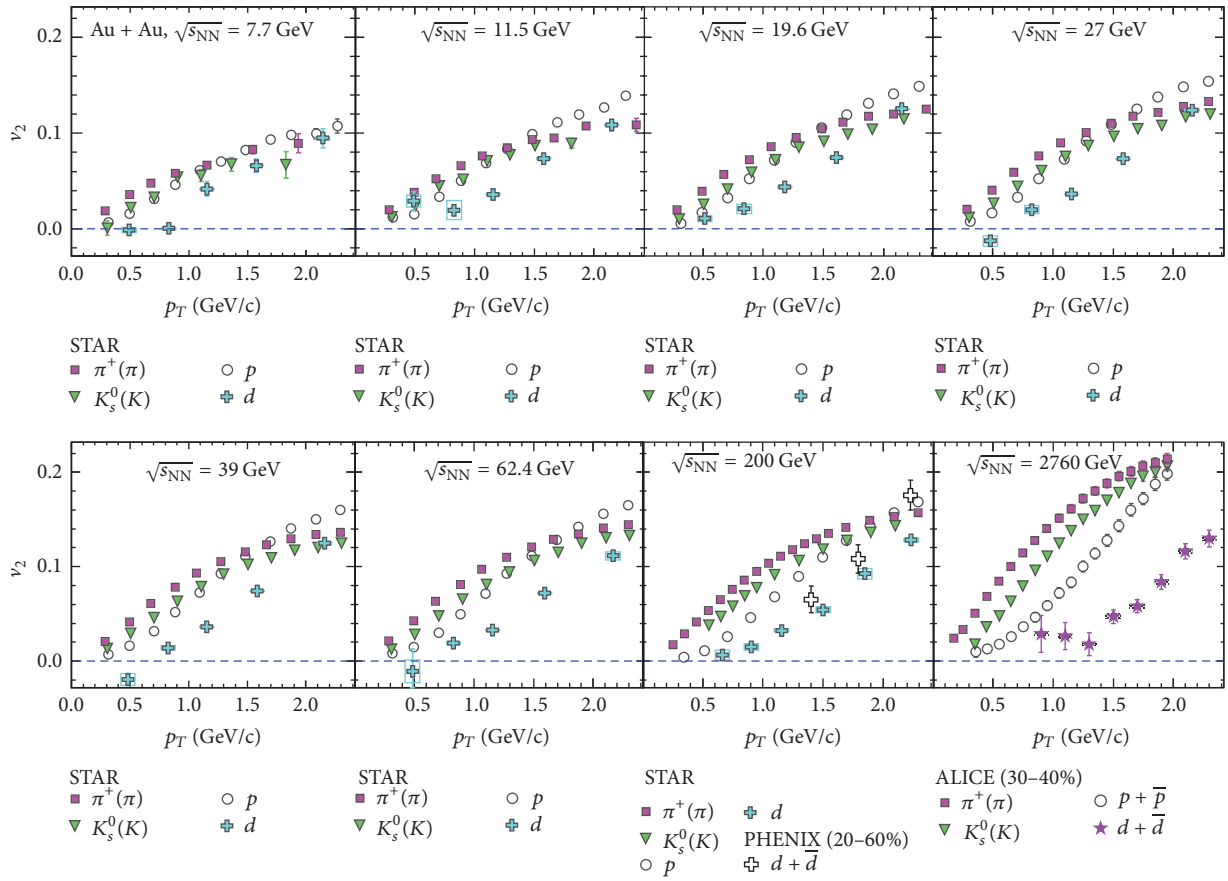

FIGURE 2: Midrapidity $v_2(p_T)$ for π^+ (squares), K^0_s (K in Pb + Pb) (triangles), p (open circles), and d (crosses) in 0–80%, 20–60%, and 30–40% centrality from STAR, PHENIX, and ALICE, respectively.

inclusive $d+\overline{d}$ v_2. The general trend of nuclei v_2 of all species is the same: it increases with increasing p_T. The slight difference of v_2 between STAR and PHENIX is due to the difference in centrality ranges. The centrality range for PHENIX is 20–60% and that for STAR is 0–80%.

From the trend in Figure 1 it seems that light nuclei v_2 show mass ordering; that is, heavier particles have smaller v_2 value compared to lighter ones, similar to v_2 of identified particles [41, 42, 44, 75]. In order to see the mass ordering effect more clearly, we restrict the x–axis range to 2.5 GeV/c and compare v_2 of d with v_2 of identified particles such as π^+, K^0_s (K in Pb + Pb), and p as shown in Figure 2. We see that d v_2 at all collision energies is lower than v_2 of the identified hadrons at a fixed value of p_T. Although mass ordering is a theoretical expectation from the hydrodynamical approach to heavy-ion collisions [76], coalescence formalism for light nuclei can also give rise to this effect. Recent studies using AMPT and VISHNU hybrid model suggest that mass ordering is also expected from transport approach to heavy-ion collisions [77–79].v_2 of light nuclei is negative for some collision energies as shown in Figure 1. This negative v_2 is expected to be the outcome of strong radial flow in heavy-ion collisions [80].

In order to study the energy dependence of light nuclei v_2, we compare the deuteron v_2 from collision energy $\sqrt{s_{NN}}$ = 7.7 GeV to 2760 GeV as shown in Figure 3. The deuteron $v_2(p_T)$ shows energy dependence prominently for high p_T ($p_T > 2.4$ GeV/c), where v_2 is highest for top collision energy ($\sqrt{s_{NN}}$ = 2760 GeV) and gradually decreases with decreasing collision energy. This energy dependent trend of light nuclei v_2 is similar to the energy dependence of identified hadron v_2 where $v_2(p_T)$ also decreases with decreasing collision energy [41, 42].

The STAR experiment has measured the difference of nuclei (d) and antinuclei ($\overline{d}$) v_2 for collision energies $\sqrt{s_{NN}}$ = 19.6, 27, 39, 62.4, and 200 GeV [63]. Figure 4 shows the difference of d and $\overline{d}$ v_2 as a function of collision energy. For comparison, the difference of proton and antiproton v_2 is also shown [41, 42]. We observe that the difference of d and $\overline{d}$ v_2 remains positive for $\sqrt{s_{NN}}$ = 7.7–39 GeV. However, for $\sqrt{s_{NN}} \geq 62.4$ GeV the difference of d and $\overline{d}$ v_2 is almost zero. The difference of d and $\overline{d}$ v_2 qualitatively follows the same trend as seen for difference of p and $\overline{p}$ v_2[41, 42]. It is easy to infer from simple coalescence model that light (anti)nuclei formed via coalescence of (anti)nucleons will also reflect similar difference in v_2 as the constituent nucleon and antinucleon. The difference in v_2 between particles and their antiparticles has been attributed to the chiral magnetic effect in finite baryon-density matter [81], different v_2 of produced

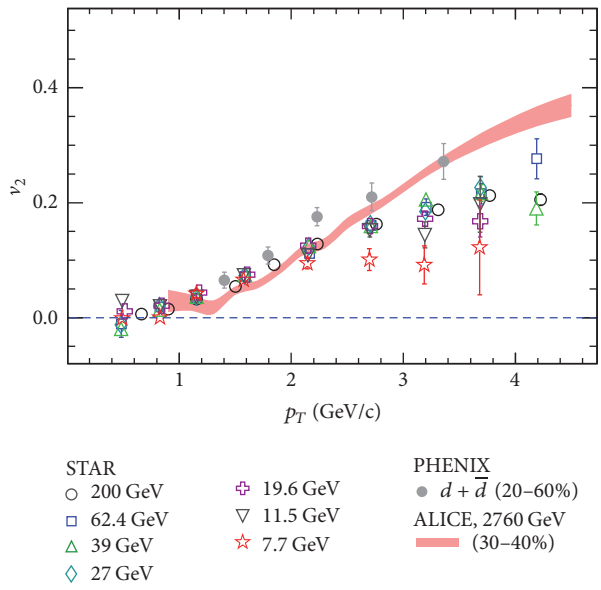

FIGURE 3: Energy dependence of midrapidity $v_2(p_T)$ of d for minimum bias (30–40% for ALICE) collisions.

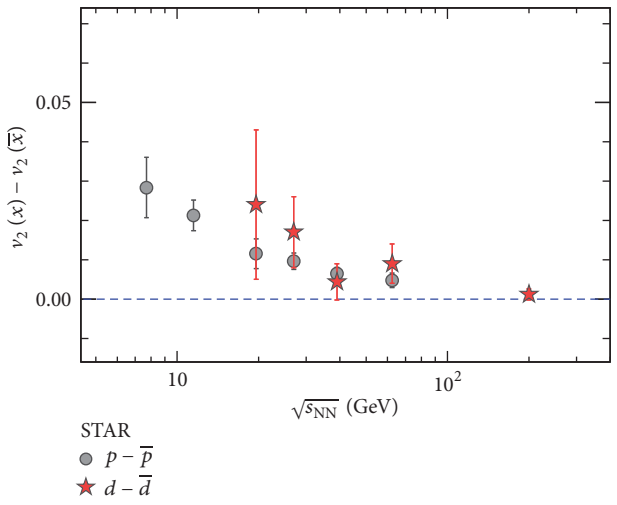

FIGURE 4: Difference of d and $\overline{d}$ $v_2(p_T)$ as a function of collision energy for minimum bias Au + Au collisions in STAR.

and transported particles [82], different rapidity distributions for quarks and antiquarks [83], the conservation of baryon number, strangeness, and isospin [84], and different mean-field potentials acting on particles and their antiparticles [85–88].

The centrality dependence of light nuclei v_2 measured by the STAR and ALICE is shown in Figure 5. STAR has measured d and $\overline{d}$ v_2 in two different centrality ranges, namely, 0–30% and 30–80% for collision energies below $\sqrt{s_{NN}}$ = 200 GeV. In case of $\sqrt{s_{NN}}$ = 200 GeV, the light nuclei v_2 are measured in three different centrality ranges, namely, 0–10% (central), 10–40% (mid-central), and 40–80% (peripheral) as high statistics data were available. ALICE has measured inclusive $d + \overline{d}$ v_2 in 6 different centrality ranges, namely, 0–5%, 5–10%, 10–20%, 20–30%, 30–40%, and 40–50%. We only present the results from 0–5%, 20–30%, and 40–50% centrality from ALICE as shown in Figure 5. v_2 of d shows strong centrality dependence for all collision energies studied in the STAR experiment. We observe that more central events have lower v_2 compared to peripheral events. $\overline{d}$ shows the same trend as d for collision energies down to $\sqrt{s_{NN}}$ = 27 GeV.

The STAR experiment could not study centrality dependence of $\overline{d}$ below $\sqrt{s_{NN}}$ = 27 GeV due to limited event statistics [63]. Comparing the centrality dependence of $d(\overline{d})$ v_2 from STAR and ALICE we can see that both experiments show strong centrality dependence of light nuclei v_2. The centrality dependence of light nuclei v_2 is analogous to the centrality dependence observed for identified nucleon $(p, \overline{p})$ v_2 [89, 90].

3.2. Mass Number Scaling and Model Comparison. It is expected from the formulations of coalescence model that if light nuclei are formed via the coalescence of nucleons then the elliptic flow of light nuclei, when divided by atomic mass number (A), should scale with the elliptic flow of nucleons [91, 92]. Therefore, we expect that the light (anti)nuclei v_2 divided by A should scale with $p(\overline{p})$ v_2. Here, we essentially assume that v_2 of (anti)proton and (anti)neutron are the same as expected from the observed NCQ scaling of identified particle v_2[41, 42]. Figure 6 shows the atomic mass number scaling of light nuclei v_2 from STAR, PHENIX, and ALICE experiments. Since ALICE does not have results in minimum bias events, we used both $p + \overline{p}$ and $d + \overline{d}$ v_2 from 30–40% centrality range. We observe that light nuclei v_2 from STAR and PHENIX show atomic mass number scaling up to $p_T/A \sim 1.5$ GeV/c. However, deviation of the scaling of the order of 20% is observed for $d + \overline{d}$ v_2 from ALICE. The scaling of light (anti)nuclei v_2 with (anti)proton v_2 suggests

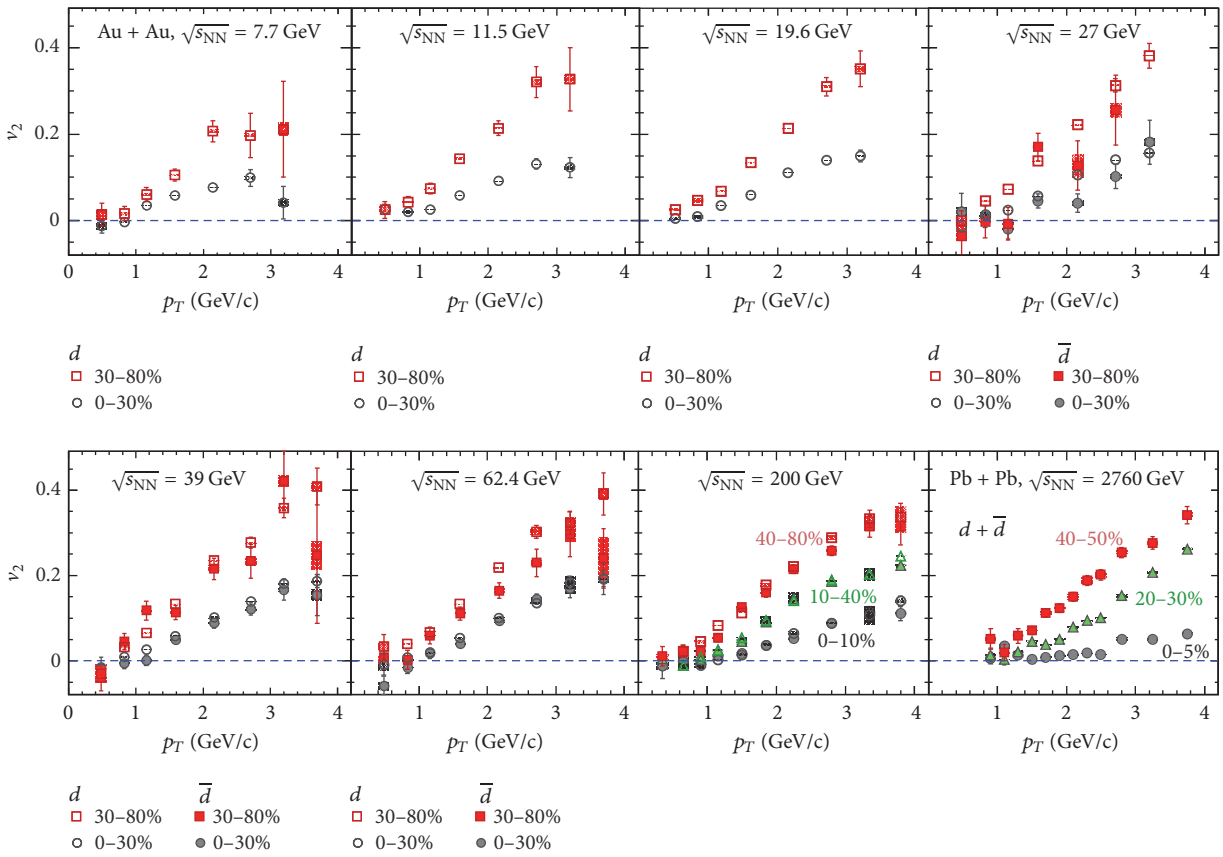

FIGURE 5: Centrality dependence of v_2 of $d(\overline{d})$ as a function of p_T.

that light (anti)nuclei might have formed via coalescence of (anti)nucleons at a later stage of the evolution at RHIC energies for p_T/A up to 1.5 GeV/c [22–32]. However, this simple picture of coalescence may not be holding for ALICE experiment at LHC energies. On the contrary, there is another method to produce light nuclei, for example, by thermal production in which it is assumed that light nuclei are produced thermally like any other primary particles [17–21]. Various thermal model studies have successfully reproduced the different ratios of produced particles as well as light nuclei in heavy-ion collisions [17–21].

In order to investigate the success of these models, both STAR and ALICE have compared the elliptic flow of light nuclei with the predictions from blast-wave models [63, 67]. Figure 7 shows the v_2 of light nuclei predicted from blast-wave model using the parameters obtained from fits to the identified particles v_2 [67, 93]. We observe that blast-wave model reproduces v_2 of light nuclei from STAR with moderate success except for low p_T (<1.0 GeV/c), where v_2 of $d(\overline{d})$ are underpredicted for all collision energies. However, the blast-wave model seems to successfully reproduce the $d + \overline{d}$ v_2 from ALICE. The low relative production of light nuclei compared to identified nucleons at RHIC collisions energies supports the procedure of light nuclei production via coalescence mechanism [22–32]. However, the success of blast-wave model in reproducing the nuclei v_2 at LHC and moderate success at RHIC suggest that the light nuclei production is also supported by thermal process [17–21]. The light nuclei production in general might be a more complicated coalescence process, for example, coalescence of nucleons in the local rest frame of the fluid cell. This scenario might give rise to deviations from simple A scaling [63].

At RHIC energies the light nuclei v_2 have been compared with results from a hybrid AMPT + coalescence model [63]. A Multiphase Transport (AMPT) model is an event generator with Glauber Monte Carlo initial state [94]. The AMPT model includes Zhang's Partonic Cascade (ZPC) model for initial partonic interactions and A Relativistic Transport (ART) model for later hadronic interactions [94]. The nucleon phase-space information from the AMPT model is fed to the coalescence model to generate light nuclei [63, 95]. Figure 8 shows the light nuclei v_2 from the coalescence model and compared to the data. The coalescence model prediction for $d + \overline{d}$ in Pb + Pb collisions at $\sqrt{s_{NN}}$ = 2760 GeV is taken from [96]. The coalescence model fairly reproduces the measurement from data for all collision energies except for the lowest energy $\sqrt{s_{NN}}$ = 7.7 GeV. The AMPT model generates nucleon v_2 from both partonic and hadronic interactions for all the collision energies presented. However, increased hadronic interactions compared to partonic, at lowest collision energies, are not implemented in the AMPT + coalescence model. This could be the reason behind the

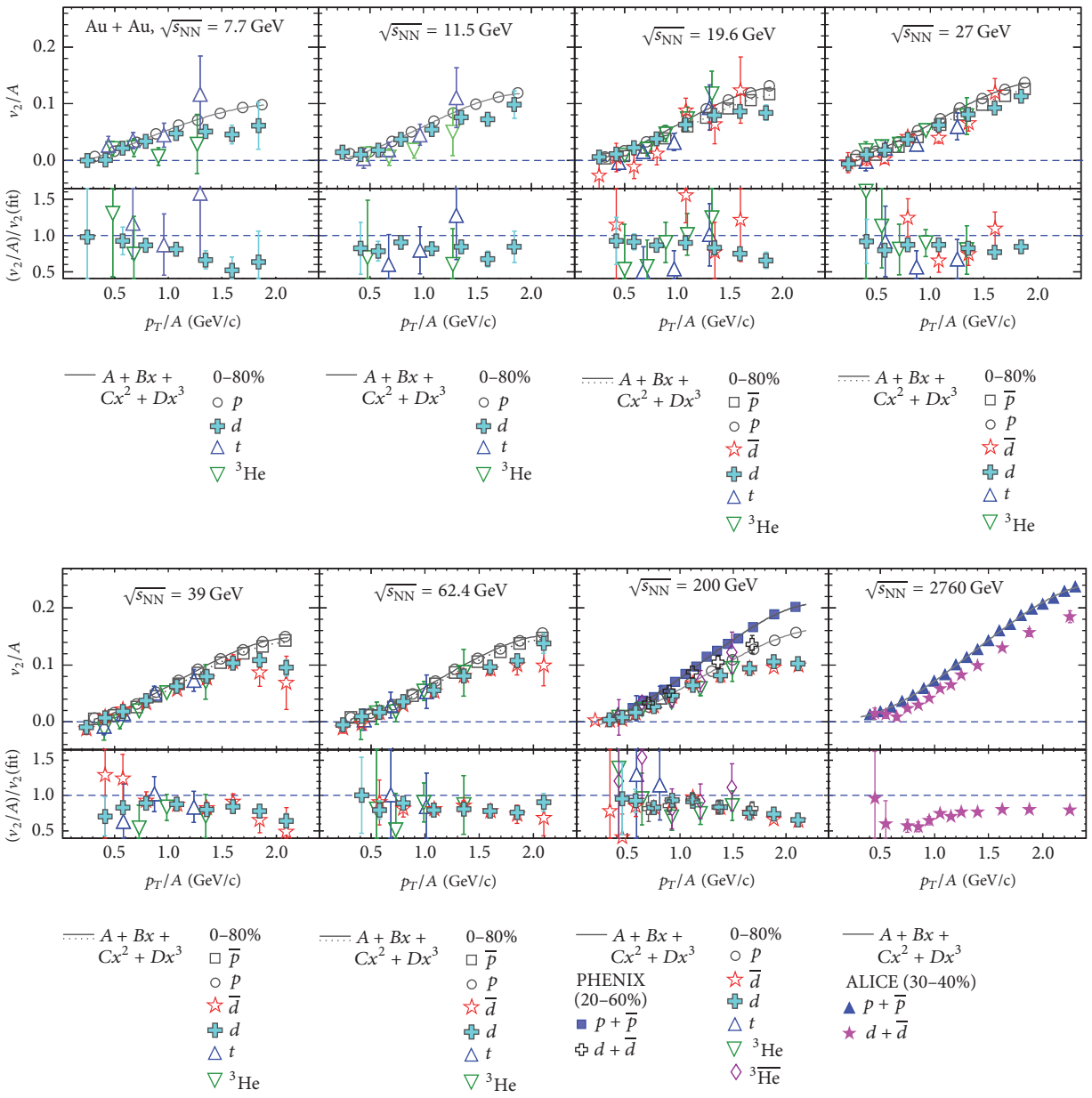

FIGURE 6: Atomic mass number scaling v_2/A of light nuclei as a function of p_T/A for STAR (0–80%), PHENIX (20–60%), and ALICE (30–40%).

deviation of the data from the model predictions at lowest collision energy [41, 42].

We have performed simultaneous fit to the v_2 and p_T spectra of identified hadrons + light nuclei using the same blast-wave model as used in [67, 75]. The simultaneous fit of v_2 and p_T spectra for measurements from the PHENIX and the ALICE experiment is shown in Figure 9. We find that the inclusion of light nuclei results to the fit does not change the fit results compared to the blast-wave fit performed only on identified hadron v_2 and p_T spectra. This indicates that the light nuclei v_2 and p_T spectra are well described by the blast-wave model.

3.3. Model Prediction of ^{3}He and ^{4}He v_2. We have predicted v_2 of ^{3}He and ^{4}He using the simple coalescence and blast-wave model. Since protons and neutrons have similar masses and the same number of constituent quarks, they should exhibit similar collective behavior and, hence, similar magnitude of v_2. Therefore, we parametrize the elliptic flow of $p + \overline{p}$ v_2 using the fit formula [97],

$$f_{v_2(p_T)}(n) = \frac{an}{1 + e^{-(p_T/n-b)/c}} - dn, \tag{14}$$

where a, b, c, and d are fit parameters and n is the constituent quark number of the particle [97]. The fit to $p + \overline{p}$ v_2 (solid

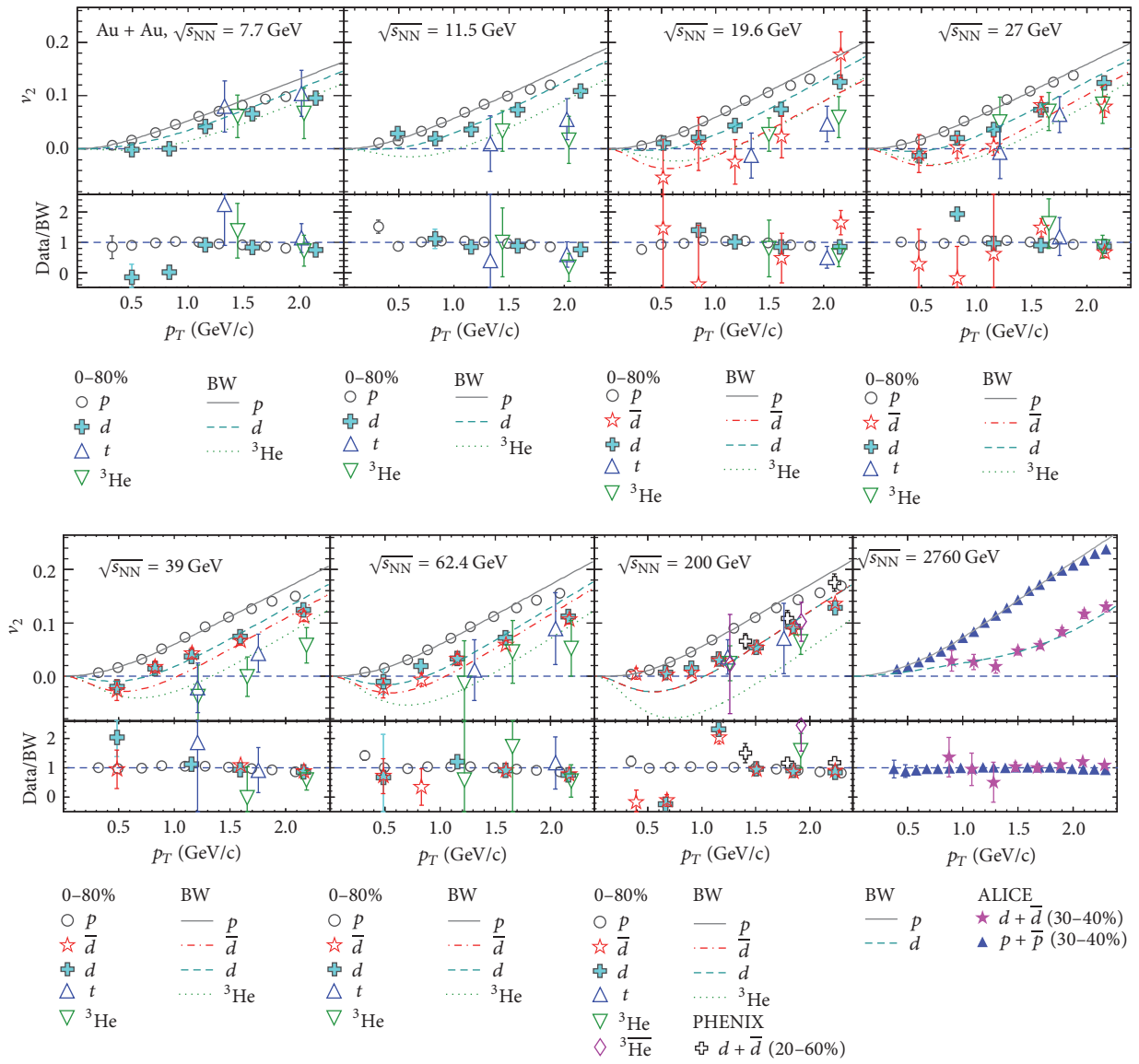

FIGURE 7: Light nuclei v_2 as a function of p_T from blast-wave model (lines). For comparison, $p + \overline{p}$ v_2 is also shown. Marker for STAR corresponds to 0–80%, PHENIX corresponds to 20–60%, and ALICE corresponds to 30–40% central events.

lines) from the PHENIX and ALICE experiment is shown in Figures 10(a) and 10(b), respectively. Assuming similar magnitude of neutron v_2 as that of proton, we then predict v_2 of ^{3}He and ^{4}He as

$$v_2\left(p_T\right)_{^3\mathrm{He}} \approx 3v_2\left(\frac{p_T}{3}\right)_p, \tag{15a}$$

$$v_2\left(p_T\right)_{^4\mathrm{He}} \approx 4v_2\left(\frac{p_T}{4}\right)_p. \tag{15b}$$

This simplified coalescence model prediction of ^{3}He and ^{4}He v_2 is shown in Figures 10(a) and 10(b) as blue (dotted and dashed) lines. For comparison, the blast-wave model predicted v_2 of ^{3}He and ^{4}He from the fit parameters obtained in Figure 9 are also shown in red (dotted and dashed) lines. We observe characteristic difference in the prediction of ^{3}He and ^{4}He v_2 from the coalescence and the blast-wave model. As one expects from the mass ordering effect of blast-wave model, v_2 of ^{3}He and ^{4}He are predicted to be almost zero in the intermediate p_T range ($1.0 < p_T < 2.5$ GeV/c). On the other hand, the simple coalescence model predicts orders of magnitude higher v_2 compared to blast-wave for both ^{3}He and ^{4}He in the same p_T range. Hence, experimental measurements of ^{3}He and ^{4}He v_2 in future would significantly improve our knowledge on the mechanisms of light nuclei formation in heavy-ion collisions [71, 98–100].

4. Summary and Conclusions

We have presented a review of elliptic flow v_2 of light nuclei (d, t, and ^{3}He) and antinuclei ($\overline{d}$ and $^3\overline{\mathrm{He}}$) from STAR experiment and inclusive $d + \overline{d}$ v_2 from PHENIX at RHIC

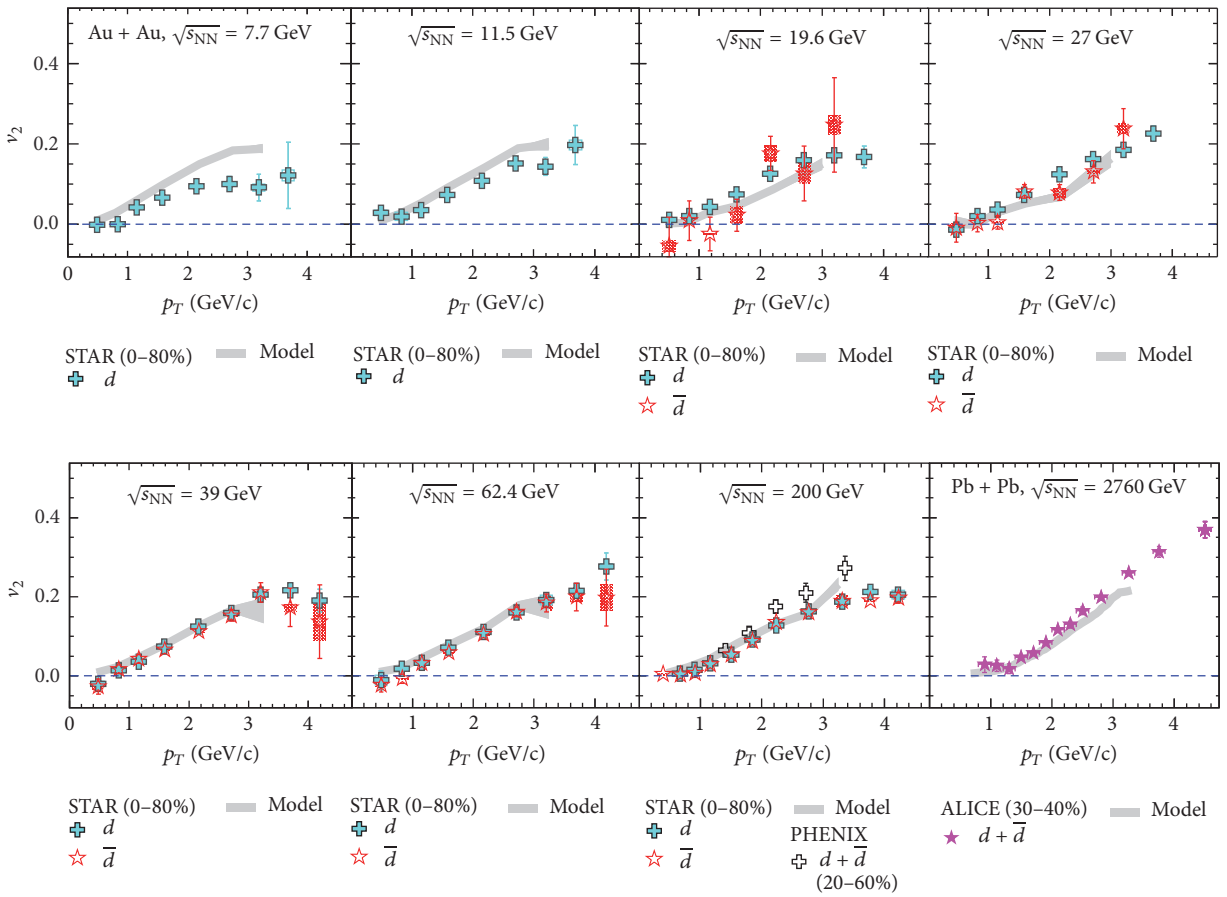

FIGURE 8: Light nuclei v_2 as a function of p_T from AMPT + coalescence model (solid lines). Marker for STAR experiment corresponds to 0–80%, PHENIX corresponds to 20–60%, and ALICE corresponds to 30–40% central events.

and ALICE at LHC. Similar to identified hadrons, the light nuclei v_2 show a monotonic rise with increasing p_T and mass ordering at low p_T for all measured collision energies. The beam energy dependence of d v_2 is small at intermediate p_T and only prominent at high p_T, which is similar to the trend as observed for the charged hadron v_2. The v_2 of nuclei and antinuclei are of similar magnitude for top collision energies at RHIC but at lower collision energies; the difference in v_2 between nuclei and antinuclei qualitatively follows the difference in proton and antiproton v_2. The centrality dependence of light (anti)nuclei $v_2(p_T)$ is similar to that of identified hadrons $v_2(p_T)$.

Light (anti)nuclei v_2 is found to follow the atomic mass number (A) scaling for almost all collision energies at RHIC suggesting coalescence as the underlying process for the light nuclei production in heavy-ion collisions. However, a deviation from mass number scaling at the level of 20% is observed at LHC. This indicates that a simple coalescence process may not be the only underlying mechanism for light nuclei production. Furthermore, a transport-plus-coalescence model study is found to approximately reproduce the light nuclei v_2 measured at RHIC and LHC. The agreement of coalescence model with the data from PHENIX and STAR is imperceptibly better than the blast-wave model. However, at the LHC energy, the light nuclei v_2 are better described by blast-wave model rather than the simple coalescence model. The coalescence mechanism, intuitively, should be the prominent process of light nuclei production. However, the breaking of mass scaling at LHC energy and success of blast-wave model prevent us from drawing any definitive conclusion on the light nuclei production mechanism.

We observed orders of magnitude difference in ^{3}He and ^{4}He v_2 as predicted by blast-wave and coalescence model. The blast-wave model predicts almost zero v_2 for ^{3}He and ^{4}He up to p_T = 2.5 GeV/c, whereas the coalescence model predicts significant v_2 for ^{3}He and ^{4}He at same p_T range. Hence, the precise measurements of ^{3}He and ^{4}He v_2 in the future can significantly improve the knowledge of the light nuclei production mechanism in heavy-ion collisions.

Conflicts of Interest

The authors declare that there are no conflicts of interest regarding the publication of this paper.

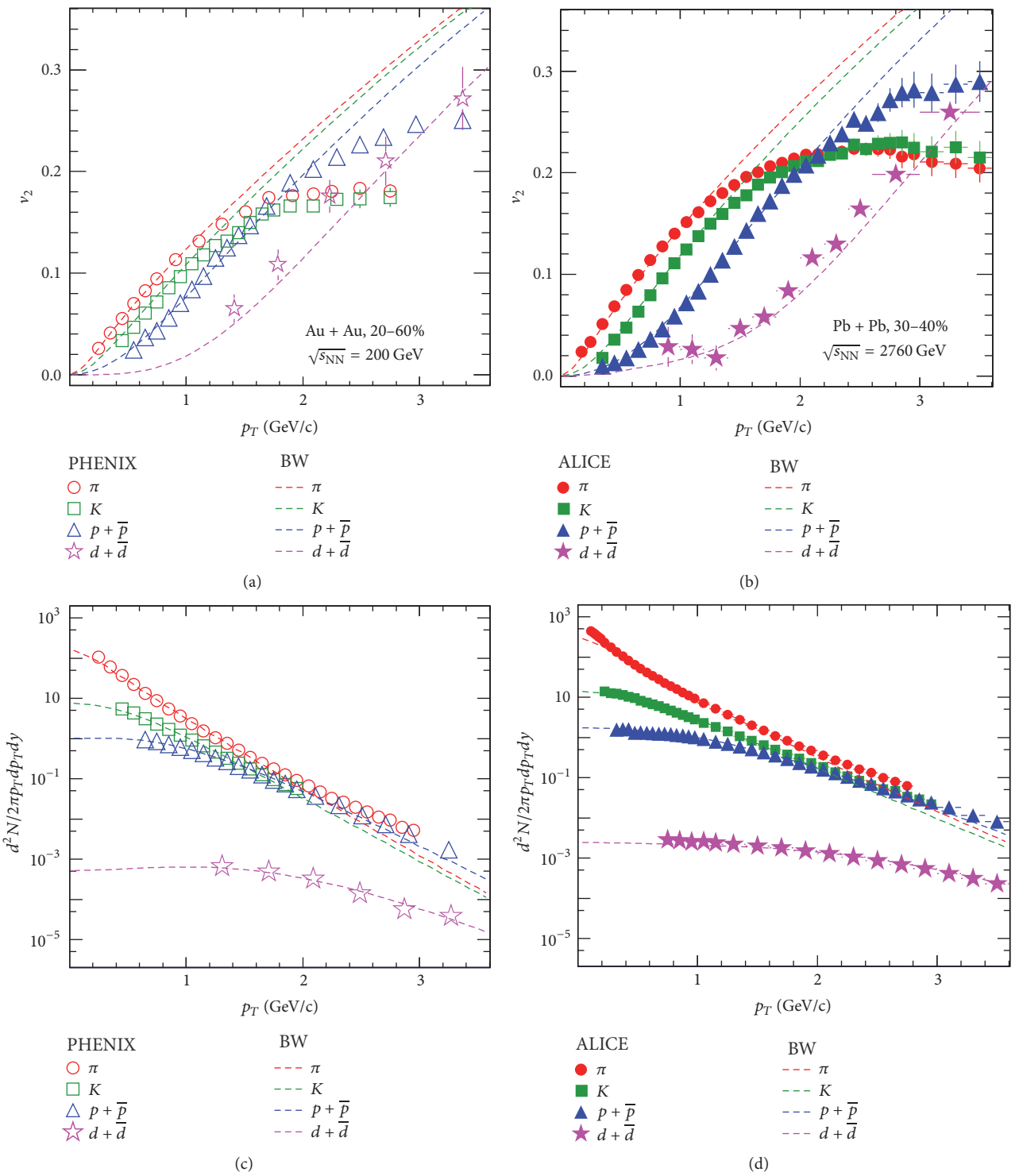

FIGURE 9: (a) Blast-wave fit of π, K, $p(\overline{p})$, $d(\overline{d})$ v_2, and (c) p_T spectra from the PHENIX experiment. The same is shown for the ALICE experiment in panels (b) and (d). p_T spectra are used from [45, 101]. Marker for PHENIX data corresponds to 20–60% and marker for ALICE data corresponds to 30–40% central events.

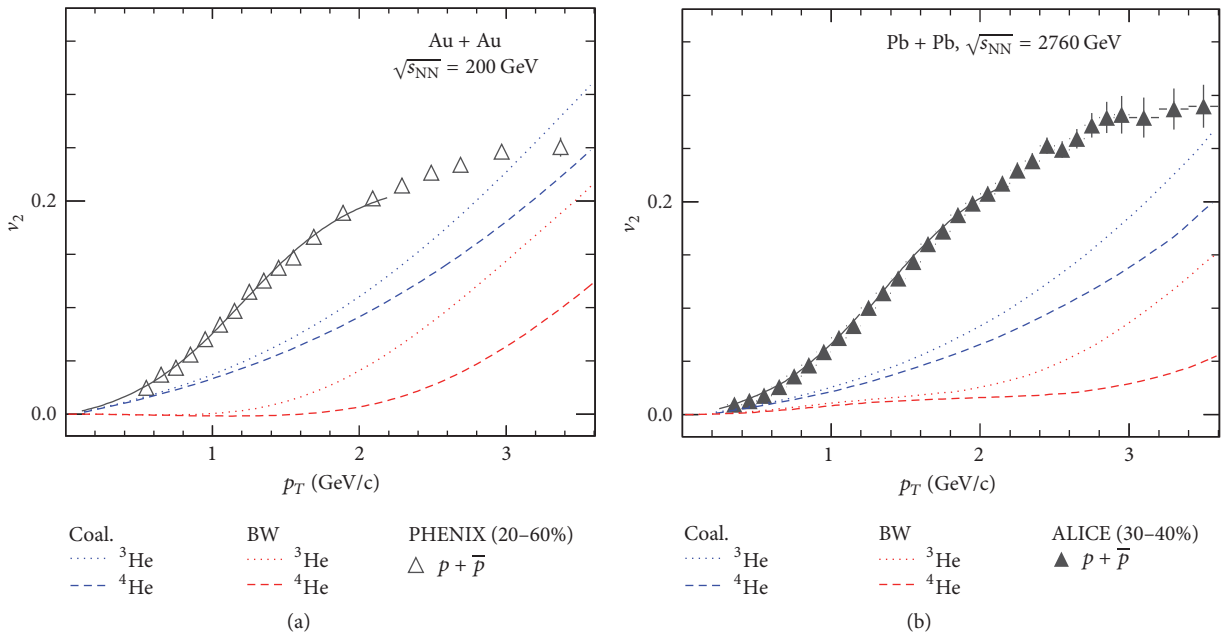

FIGURE 10: (a) Coalescence model predictions (blue lines) of ^{3}He and ^{4}He v_2 for (a) $\sqrt{s_{NN}}$ = 200 GeV and (b) for $\sqrt{s_{NN}}$ = 2760 GeV. The blast-wave predictions of ^{3}He and ^{4}He v_2 are also shown in red lines.

Acknowledgments

The authors thank STAR collaboration, PHENIX collaboration, and ALICE collaboration for providing the light nuclei v_2 data and the model predictions. This work is supported by DAE-BRNS Project (Grant no. 2010/21/15-BRNS/2026) and Dr. C. Jena is supported by 12th plan project (PIC no. 12-R&D-NIS-5.11-0300).

References

[1] M. Stephanov, K. Rajagopal, and E. Shuryak, "Signatures of the tricritical point in QCD," *Physical Review Letters*, vol. 81, no. 22, pp. 4816–4819, 1998.

[2] M. A. Stephanov, K. Rajagopal, and E. V. Shuryak, "Event-by-event fluctuations in heavy ion collisions and the QCD critical point," *Physical Review D*, vol. 60, Article ID 114028, 1999.

[3] M. A. Stephanov, "QCD phase diagram: an overview," https://arxiv.org/abs/hep-lat/0701002.

[4] K. Fukushima and T. Hatsuda, "The phase diagram of dense QCD," *Reports on Progress in Physics*, vol. 74, no. 1, Article ID 014001, 2010.

[5] I. Arsene, Bearden. I. G., D. Beavis et al., "Quark–gluon plasma and color glass condensate at RHIC? The perspective from the BRAHMS experiment," *Nuclear Physics A*, vol. 757, no. 1-2, pp. 1–27, 2005.

[6] B. B. Back, M. D. Baker, M. Ballintijn et al., "The PHOBOS perspective on discoveries at RHIC," *Nuclear Physics A*, vol. 757, pp. 28–101, 2005.

[7] J. Adams, M. M. Aggarwal, Z. Ahammed et al., "Experimental and theoretical challenges in the search for the quark–gluon plasma: The STAR Collaboration's critical assessment of the evidence from RHIC collisions," *Nuclear Physics A*, vol. 757, no. 1–2, pp. 102–183, 2005.

[8] K. Adcox, S. S. Adler, S. Afanasiev et al., "Formation of dense partonic matter in relativistic nucleus–nucleus collisions at RHIC: experimental evaluation by the PHENIX Collaboration," *Nuclear Physics A*, vol. 757, no. 1-2, pp. 184–283, 2005.

[9] S. Gupta, X. Luo, B. Mohanty, H. G. Ritter, and N. Xu, "Scale for the phase diagram of quantum chromodynamics," *Science*, vol. 332, no. 6037, pp. 1525–1528, 2011.

[10] L. Adamczyk, J. K. Adkins, G. Agakishiev et al., "Energy dependence of moments of net-proton multiplicity distributions at RHIC," *Physical Review Letters*, vol. 112, Article ID 032302, 2014.

[11] N. Itoh, "Hydrostatic equilibrium of hypothetical quark stars," *Progress of Theoretical Physics*, vol. 44, no. 1, pp. 291-292, 1970.

[12] K. Aamodt, A. Abrahantes Quintana, R. Achenbach et al., "The ALICE experiment at the CERN LHC," *Journal of Instrumentation*, vol. 3, Article ID S08002, 2008.

[13] B. B. Abelev, J. Adam, D. Adamová et al., "Performance of the ALICE experiment at the CERN LHC," *International Journal of Modern Physics A*, vol. 29, no. 24, article 120, Article ID 1430044, 2014.

[14] G. Lemaître, "Un Univers homogène de masse constante et de rayon croissant rendant compte de la vitesse radiale des nébuleuses extra-galactiques," *Annales de la société Scientifique de Bruxelles*, vol. 47, pp. 49–59, 1927.

[15] A. Z. Mekjian, "Explosive nucleosynthesis, equilibrium thermodynamics, and relativistic heavy-ion collisions," *Physical Review C*, vol. 17, article 1051, 1978.

[16] P. Siemens and J. I. Kapusta, "Evidence for a soft nuclear-matter equation of state," *Physical Review Letters*, vol. 43, article 1486, 1979.

[17] P. Braun-Munzinger and J. Stachel, "Production of strange clusters and strange matter in nucleus-nucleus collisions at the AGS," *Journal of Physics G: Nuclear and Particle Physics*, vol. 21, no. 3, article L17, 1995.

[18] P. Braun-Munzinger and J. Stachel, "Particle ratios, equilibration and the QCD phase boundary," *Journal of Physics G: Nuclear and Particle Physics*, vol. 28, no. 7, article 1971, 2002.

[19] A. Andronic, P. Braun-Munzinger, J. Stachel, and H. Stocker, "Production of light nuclei, hypernuclei and their antiparticles in relativistic nuclear collisions," *Physics Letters B*, vol. 697, no. 3, pp. 203–207, 2011.

[20] J. Stachel, A. Andronic, P. Braun-Munzinger, and K. Redlich, "Confronting LHC data with the statistical hadronization model," *Journal of Physics: Conference Series*, vol. 509, no. 1, Article ID 01201, 2014.

[21] S. Chatterjee and B. Mohanty, "Production of light nuclei in heavy-ion collisions within a multiple-freezeout scenario," *Physical Review C*, vol. 90, Article ID 034908, 2014.

[22] S. T. Butler and C. A. Pearson, "Deuterons from high-energy proton bombardment of matter," *Physical Review Letters*, vol. 129, no. 836, 1963.

[23] A. Schwarzschild and A. Zupancic, "Production of Tritons, Deuterons, Nucleons, and Mesons by 30-GeV Protons on A1, Be, and Fe targets," *Physical Review Letters*, vol. 129, no. 2, pp. 854–862, 1963.

[24] H. H. Gutbrod, A. Sandoval, P. J. Johansen et al., "Final-state interactions in the production of hydrogen and helium isotopes by relativistic heavy ions on uranium," *Physical Review Letters*, vol. 37, 667 pages, 1976.

[25] H. Sato and K. Yazaki, "On the coalescence model for high energy nuclear reactions," *Physics Letters B*, vol. 98, no. 3, pp. 153–157, 1981.

[26] E. A. Remler, "Composite particle cross sections from the density operator," *Annals of Physics*, vol. 136, no. 2, pp. 293–316, 1981.

[27] M. Gyulassy, K. Frankel, and E. A. Remler, "Deuteron formation in nuclear collisions," *Nuclear Physics A*, vol. 402, no. 3, pp. 596–611, 1983.

[28] L. Csernai and J. I. Kapusta, "Entropy and cluster production in nuclear collisions," *Physics Reports*, vol. 131, no. 4, pp. 223–318, 1986.

[29] P. Danielewicz and G. F. Bertsch, "Production of deuterons and pions in a transport model of energetic heavy-ion reactions," *Nuclear Physics A*, vol. 533, no. 4, pp. 712–748, 1991.

[30] C. B. Dover, U. Heinz, E. Schnedermann, and J. Zimnyi, "Covariant coalescence model for relativistically expanding systems," *Physical Review C*, vol. 44, no. 4, pp. 1636–1654, 1991.

[31] W. J. Llope, S. E. Pratt, N. Frazier et al., "The fragment coalescence model," *Physical Review C*, vol. 52, article 2004, 1995.

[32] J. L. Nagle, B. S. Kumar, D. Kusnezov, H. Sorge, and R. Mattiello, "Coalescence of deuterons in relativistic heavy ion collisions," *Physical Review C*, vol. 53, no. 1, pp. 367–376, 1996.

[33] R. Scheibl and U. Heinz, "Coalescence and flow in ultrarelativistic heavy ion collisions," *Physical Review C*, vol. 59, article 1585, 1999.

[34] S. Zhang, J. Chen, H. Crawford, D. Keane, Y. Ma, and Z. B. Xu, "Searching for onset of deconfinement via hypernuclei and baryon-strangeness correlations," *Physics Letters B*, vol. 684, no. 4-5, pp. 224–227, 2010.

[35] J. Steinheimer, K. Gudima, A. Botvina, I. Mishustin, M. Bleicher, and H. Stöcker, "Hypernuclei, dibaryon and antinuclei production in high energy heavy ion collisions: thermal production vs. coalescence," *Physics Letters B*, vol. 714, no. 1, pp. 85–91, 2012.

[36] S. Mrówczyński, "Production of light nuclei in the thermal and coalescence models," *Acta Physica Polonica B*, vol. 48, no. 4, p. 707, 2017.

[37] V. I. Voloshin, "Anisotropic flow," *Nuclear Physics A*, vol. 715, pp. 379c–388c, 2003.

[38] D. Molnar and S. A. Voloshin, "Elliptic flow at large transverse momenta from quark coalescence," *Physical Review Letters*, vol. 91, Article ID 092301, 2003.

[39] R. C. Hwa and C. B. Yang, "Scaling distributions of quarks, mesons, and proton for all PT energy, and centrality," *Physical Review C*, vol. 67, no. 6, Article ID 064902, 2003.

[40] R. J. Fries, B. Muller, C. Nonaka, and S. A. Bass, "Hadronization in heavy-ion collisions: recombination and fragmentation of partons," *Physical Review Letters*, vol. 90, Article ID 202303, 2003.

[41] L. Adamczyk, J. K. Adkins, G. Agakishiev et al., "Elliptic flow of identified hadrons in Au+Au collisions at $\sqrt{sNN} = 7.7 - 62.4$ GeV," *Physical Review C*, vol. 88, Article ID 014902, 2013.

[42] L. Adamczyk, J. K. Adkins, G. Agakishiev et al., "Observation of an energy-dependent difference in elliptic flow between particles and anti-particles in relativistic heavy ion collisions," *Physical Review Letters*, vol. 110, Article ID 142301, 2013.

[43] L. Adamczyk, J. K. Adkins, G. Agakishiev et al., "Centrality and transverse momentum dependence of elliptic flow of multistrange hadrons and Ø Meson in Au + Au Collisions at $\sqrt{s\mathrm{NN}} = 200$ GeV," *Physical Review Letters*, vol. 116, no. 6, Article ID 062301, 2016.

[44] S. S. Adler, Z. Ahammed, C. Allgower et al., "Identified particle elliptic flow in Au+Au collisions at $\sqrt{s\mathrm{NN}} = 200$ GeV," *Physical Review Letters*, vol. 91, Article ID 182301, 2003.

[45] S. S. Adler, S. Afanasiev, C. Aidala et al., "Identified charged particle spectra and yields in Au+Au collisions at $\sqrt{s\mathrm{NN}} = 200$ GeV," *Physical Review C*, vol. 69, Article ID 034909, 2004.

[46] S. Nagamiya, M.-C. Lemaire, E. Moeller et al., "Production of pions and light fragments at large angles in high-energy nuclear collisions," *Physical Review C*, vol. 24, article 971, 1981.

[47] R. L. Auble, J. B. Ball, F. E. Bertrand et al., "Light ion emission from reactions induced by 0.8–2.4 GeV ^{16}O projectiles," *Physical Review C*, vol. 28, article 1552, 1983.

[48] S. Wang, S. Albergo, F. Bieser et al., "Light fragment production and power law behavior in Au + Au collisions," *Physical Review Letters*, vol. 74, article 2646, 1995.

[49] M. A. Lisa, S. Albergo, F. Bieser et al., "Radial flow in Au + Au collisions at $E = (0.25 - 1.15)$ A GeV," *Physical Review Letters*, vol. 75, article 2662, 1995.

[50] M. Aoki, J. Beatty, D. Beavis et al., "Measurements at 0° of negatively charged particles and antinuclei produced in collisions of 14.6A GeV/c Si on Al, Cu, and Au targets," *Physical Review Letters*, vol. 69, article 2345, 1992.

[51] T. A. Armstrong, K. N. Barish, S. Batsouli et al., "Antideuteron yield at the AGS and coalescence implications," *Physical Review Letters*, vol. 85, article 2685, 2000.

[52] J. Barrette, R. Bellwied, S. Bennett et al., "Light fragment yields from central Au+Au collisions at 11.5A GeV/c," *Physical Review C*, vol. 61, Article ID 044906, 2000.

[53] S. Albergo, R. Bellwied, M. Bennett et al., "Light nuclei production in heavy-ion collisions at relativistic energies," *Physical Review C*, vol. 65, Article ID 034907, 2002.

[54] S. Kabana, G. Ambrosini, R. Arsenescu et al., "New results from NA52 on particle production in Pb+Pb collisions at 158 GeV per nucleon," *Nuclear Physics A*, vol. 638, no. 1-2, pp. 411c–414c, 1998.

[55] T. Anticic, R. Snellings, and S. Voloshin, "Flow analysis with cumulants: direct calculations," *Physical Review C*, vol. 85, Article ID 044913, 2012.

[56] G. L. Melkumov, "Recent results on (anti)nucleus and (anti)hyperon production in nucleus-nucleus collisions at CERN SPS energies," PoS(CPOD07), 024, 2007.

[57] V. I. Kolesnikov, "Anti-nuclei and nuclei production in Pb+Pb collisions at CERN SPS energies," *Journal of Physics: Conference Series*, vol. 110, no. 3, Article ID 032010, 2008.

[58] I. G. Bearden, H. Bøggild, J. G. Boissevain, and A. Ljubicic, "Antideuteron production in 158 *A* GeV/*c* Pb+Pb collisions," *Physical Review Letters*, vol. 85, article 2681, 2000.

[59] A. Polleri, J. P. Bondorf, I. N. Mishustin et al., "Effects of collective expansion on light cluster spectra in relativistic heavy ion collisions," *Physics Letters B*, vol. 419, pp. 19–24, 1998.

[60] S. Voloshin and Y. Zhang, "Flow study in relativistic nuclear collisions by Fourier expansion of azimuthal particle distributions," *Zeitschrift für Physik C Particles and Fields*, vol. 70, no. 4, pp. 665–671, 1996.

[61] A. M. Poskanzer and S. A. Voloshin, "Methods for analyzing anisotropic flow in relativistic nuclear collisions," *Physical Review C*, vol. 58, article 1671, 1998.

[62] P. Danielewicz, "Effects of compression and collective expansion on particle emission from central heavy-ion reactions," *Physical Review C*, vol. 51, article 716, 1995.

[63] L. Adamczyk, J. K. Adkins, G. Agakishiev et al., "Measurement of elliptic flow of light nuclei at $\sqrt{s_{\mathrm{NN}}}$ = 200, 62.4, 39, 27, 19.6, 11.5, and 7.7 GeV at the BNL relativistic heavy ion collider," *Physical Review C*, vol. 94, Article ID 034908, 2016.

[64] J. Barrette et al., "Proton and pion production relative to the reaction plane in Au + Au collisions at 11 *A* GeV/*c*," *Physical Review C*, vol. 56, article 3254, 1997.

[65] J. Barrette, R. Bellwied, S. Bennett et al., "Energy and charged particle flow in 10.8 *A* GeV/*c* Au+Au collisions," *Physical Review C*, vol. 55, article 1420, 1997.

[66] S. Afanasiev et al., "Elliptic Flow for ϕ Mesons and (Anti)deuterons in Au + Au Collisions at $\sqrt{sNN}$ = 200 GeV," *Physical Review Letters*, vol. 99, Article ID 052301, 2007.

[67] S. Acharya, D. Adamová, J. Adolfsson et al., "Measurement of deuteron spectra and elliptic flow in Pb-Pb collisions at $\sqrt{s_{\mathrm{NN}}}$ = 2.76 TeV at the LHC," https://arxiv.org/abs/1707.07304.

[68] M. Anderson, J. Berkovitz, W. Betts et al., "The STAR time projection chamber: a unique tool for studying high multiplicity events at RHIC," *Nuclear Instruments and Methods in Physics Research Section A*, vol. 499, pp. 659–678, 2003.

[69] J. Adams, M. M. Aggarwal, Z. Ahammed et al., "Identified hadron spectra at large transverse momentum in p + p and d + Au collisions at $\sqrt{sNN}$ = 200 GeV," *Physics Letters B*, vol. 637, pp. 161–169, 2006.

[70] J. Alme, Y. Andres, H. Appelshäuser et al., "The ALICE TPC, a large 3-dimensional tracking device with fast readout for ultra-high multiplicity events," *Nuclear Instruments and Methods in Physics Research Section A*, vol. 622, pp. 316–367, 2010.

[71] J. Adam, D. Adamová, M. M. Aggarwal et al., "Production of light nuclei and anti-nuclei in pp and Pb-Pb collisions at LHC energies," *Physical Review C*, vol. 93, Article ID 024917, 2016.

[72] W. J. Llope and STAR TOF Group, "The large-area time-of-flight upgrade for STAR," *Nuclear Instruments and Methods in Physics Research Section B: Beam Interactions with Materials and Atoms*, vol. 241, p. 306, 2005.

[73] W. J. Llope, "Multigap RPCs in the STAR experiment at RHIC," *Nuclear Instruments and Methods in Physics Research A*, vol. 661, pp. S110–S113, 2012.

[74] A. Akindinov, A. Alici, A. Agostinelli et al., "Performance of the ALICE time-of-flight detector at the LHC," *The European Physical Journal Plus*, vol. 128, no. 44, 2013.

[75] B. Abelev, J. Adam, D. Adamová et al., "Elliptic flow of identified hadrons in Pb-Pb collisions at $\sqrt{sNN}$ = 2.76 TeV," *Journal of High Energy Physics*, vol. 2015, article 190, 2015.

[76] P. Huovinen, P. F. Kolb, U. W. Heinz, P. V. Ruuskanen, and S. A. Voloshin, "Radial and elliptic flow at RHIC: further predictions," *Physics Letters B*, vol. 503, no. 1-2, pp. 58–64, 2001.

[77] H. Li, L. He, Z.-W. Lin, D. Molnar, F. Wang, and W. Xie, "Origin of the mass splitting of elliptic anisotropy in a multiphase transport model," *Physical Review C*, vol. 93, Article ID 051901, 2016.

[78] H. Li, L. He, Z.-W. Lin, D. Molnar, F. Wang, and W. Xie, "Origin of the mass splitting of azimuthal anisotropies in a multi-phase transport model," https://arxiv.org/abs/1604.07387.

[79] H. Xu, Z. Li, and H. Song, "High-order flow harmonics of identified hadrons in 2.76 *A* TeV Pb + Pb collisions," *Physical Review C*, vol. 93, Article ID 064905, 2016.

[80] S. A. Voloshin, A. M. Poskanzer, and R. Snellings, *Collective Phenomena in Non-Central Nuclear Collisions*, vol. 23 of *Landolt-Börnstein Series*, Springer, Berlin, Germany, 2010.

[81] Y. Burnier, D. E. Kharzeev, J. Liao, and H. U. Yee, "Chiral magnetic wave at finite baryon density and the electric quadrupole moment of the quark-gluon plasma," *Physical Review Letters*, vol. 107, Article ID 052303, 2011.

[82] J. C. Dunlop, M. A. Lisa, and P. Sorensen, "Constituent quark scaling violation due to baryon number transport," *Physical Review C*, vol. 84, Article ID 044914, 2011.

[83] V. Greco, M. Mitrovski, and G. Torrieri, "Elliptic flow in heavy ion collisions at varying energies: partonic versus hadronic dynamics," *Physical Review C*, vol. 86, Article ID 044905, 2012.

[84] J. Steinheimer, V. Koch, and M. Bleicher, "Hydrodynamics at large baryon densities: understanding proton versus anti-proton v_2 and other puzzles," *Physical Review C*, vol. 86, Article ID 044903, 2012.

[85] J. Xu, L. W. Chen, C. M. Ko, and Z. W. Lin, "Effects of hadronic potentials on elliptic flows in relativistic heavy ion collisions," *Physical Review C*, vol. 85, Article ID 041901, 2012.

[86] J. Xu, T. Song, C. M. Ko, and F. Li, "Elliptic flow splitting as a probe of the QCD phase structure at finite baryon chemical potential," *Physical Review Letters*, vol. 112, Article ID 012301, 2014.

[87] T. Song, S. Plumari, V. Greco, C. M. Ko, and F. Li, "Partonic mean-field effects on matter and antimatter elliptic flows," https://arxiv.org/abs/1211.5511.

[88] J. Xu, C. M. Ko, F. Li, T. Song, and H. Liu, "Mean-field potential effects on particle and antiparticle elliptic flows in the beam-energy scan program at RHIC," *Nuclear Physics Review*, vol. 32, article 146, 2015.

[89] L. Adamczyk, J. K. Adkins, G. Agakishiev et al., "Centrality dependence of identified particle elliptic flow in relativistic heavy ion collisions at $\sqrt{sNN}$ = 7.7 – 62.4 GeV," *Physical Review C*, vol. 93, Article ID 014907, 2016.

[90] B. Abelev, J. Adam, D. Adamová et al., "Elliptic flow of identified hadrons in Pb-Pb collisions at $\sqrt{sNN}$ = 2.76 TeV," *Journal of High Energy Physics*, vol. 2015, article 190, 190 pages, 2015.

[91] T. Z. Yan, Y. G. Ma, X. Z. Cai et al., "Scaling of anisotropic flow and momentum-space densities for light particles in intermediate energy heavy ion collisions," *Physics Letters B*, vol. 638, no. 1, pp. 50–54, 2006.

[92] Y. Oh and C. M. Ko, "Elliptic flow of deuterons in relativistic heavy-ion collisions," *Physical Review C - Nuclear Physics*, vol. 76, no. 5, Article ID 054910, 2007.

[93] X. Sun, H. Masui, A. M. Poskanzer, and A. Schmah, "Blast wave fits to elliptic flow data at $\sqrt{s_{\mathrm{NN}}}$ = 7.7–2760 GeV," *Physical Review C*, vol. 91, Article ID 024903, 2015.

[94] Z. Lin, C. M. Ko, B. A. Li, B. Zhang, and S. Pal, "Multiphase transport model for relativistic heavy ion collisions," *Physical Review C*, vol. 72, Article ID 064901, 2005.

[95] M. R. Haque, *Nuclei production and azimuthal anisotropy of charged particles in heavy-ion collisions at RHIC [Ph.D Thesis]*, NISER India, https://drupal.star.bnl.gov/STAR/theses/phd-67.

[96] L. Zhu, C. M. Ko, and X. Yin, "Light (anti-)nuclei production and flow in relativistic heavy-ion collisions," *Physical Review C*, vol. 92, no. 6, Article ID 064911, 2015.

[97] X. Dong, S. Esumi, P. Sorensen, N. Xu, and Z. Xu, "Resonance decay effects on anisotropy parameters," *Physics Letters B*, vol. 597, no. 3-4, pp. 328–332, 2004.

[98] H. Agakishiev, A. V. Alakhverdyants, G. S. Averichev et al., "Observation of the antimatter helium-4 nucleus," *Nature*, vol. 473, pp. 353–356, 2011.

[99] B. I. Abelev, M. M. Aggarwal, and Z. Ahammed, "Observation of an antimatter hypernucleus," *Science*, vol. 328, no. 5974, pp. 58–62, 2010.

[100] J. Adam, D. Adamová, M. M. Aggarwal et al., "${}^{3}_{A}H$ and production in Pb–Pb collisions at $\sqrt{sNN}$ = 2.76 TeV," *Physics Letters B*, vol. 754, pp. 360–372, 2016.

[101] B. Abelev, J. Adam, D. Adamová et al., "Production of charged pions, kaons and protons at large transverse momenta in *pp* and Pb-Pb collisions at $\sqrt{sNN}$ = 2.76 TeV," *Physics Letters B*, vol. 736, pp. 196–207, 2014.